Braiding DNA: Experiments, Simulations, and Models

G. Charvin,* A. Vologodskii,† D. Bensimon,* and V. Croquette*
*Laboratoire de Physique Statistique, Ecole Normale Supérieure, UMR 8550, Centre National de la Recherche Scientifique, Paris, France; and †Department of Chemistry, New York University, New York, New York

ABSTRACT DNA encounters topological problems in vivo because of its extended double-helical structure. As a consequence, the semiconservative mechanism of DNA replication leads to the formation of DNA braids or catenanes, which have to be removed for the completion of cell division. To get a better understanding of these structures, we have studied the elastic behavior of two braided nicked DNA molecules using a magnetic trap apparatus. The experimental data let us identify and characterize three regimes of braiding: a slightly twisted regime before the formation of the first crossing, followed by genuine braids which, at large braiding number, buckle to form plectonemes. Two different approaches support and quantify this characterization of the data. First, Monte Carlo (MC) simulations of braided DNAs yield a full description of the molecules' behavior and their buckling transition. Second, modeling the braids as a twisted swing provides a good approximation of the elastic response of the molecules as they are intertwined. Comparisons of the experiments and the MC simulations with this analytical model allow for a measurement of the diameter of the braids and its dependence upon entropic and electrostatic repulsive interactions. The MC simulations allow for an estimate of the effective torsional constant of the braids (at a stretching force $F = 2$ pN): $C_b \sim 48$ nm (as compared with $C \sim 100$ nm for a single unnicked DNA). Finally, at low salt concentrations and for sufficiently large number of braids, the diameter of the braided molecules is observed to collapse to that of double-stranded DNA. We suggest that this collapse is due to the partial melting and fraying of the two nicked molecules and the subsequent right- or left-handed intertwining of the stretched single strands.

INTRODUCTION

The helical structure of double-stranded DNA and the semiconservative mechanism (Meselson and Stahl, 1958) of DNA replication pose significant topological constraints upon DNA (Watson and Crick, 1953): if nothing is done to separate the newly synthesized strands, they remain catenated and the process of cell division is stopped. Furthermore, the progression of the replication complex induces a torsional constraint in the DNA molecule, which leads to the formation of supercoils (Wang, 2002; Schvartzman and Stasiak, 2004). A class of enzymes, called topoisomerases, is in charge of resolving these constraints. These enzymes are divided into two types: type I and type II (Wang et al., 1998). Type II topoisomerases use ATP to induce topological changes in DNA. They transiently cut a DNA segment (the gate), and pass another segment through that cut before relegating the gate segment. Using this mechanism, they can either relax the positive supercoils generated ahead of the replication fork or unlink the intertwined daughter DNAs behind. Although twisting a single DNA molecule offers an interesting in vitro model for supercoiling, the braiding of two molecules is relevant to an understanding of the structure of the replication intermediates.

Whereas the behavior of a single DNA molecule under torsion has been extensively investigated experimentally (Strick et al., 1996; Cluzel et al., 1996; Leger et al., 1998; Bryant et al., 2003), numerically (Vologodskii and Cozzarelli, 1996; Vologodskii and Marko, 1997), and theoretically (Bouchiat and Mézard, 1998; Marko and Siggia, 1995; Marko, 1997; Moroz and Nelson, 1998a,b), there are but a few experiments or models (Marko, 1997, 1999) dealing with the braiding of two molecules. Preliminary experiments (Strick et al., 1998) have revealed the existence of different regimes of braiding but did not allow for a comprehensive interpretation of them. More recent studies have suggested that DNA braids could form plectonemic structures (Charvin et al., 2003; Stone et al., 2003), but did not provide direct evidence of their existence.

In this article, we report an exhaustive experimental and numerical study of the elastic properties of a braid that consists of two intertwined nicked double-stranded DNAs. At high catenation number, the experiment suggests that the twisted braids undergo a mechanical instability that leads to the formation of plectonemic structures. Monte Carlo (MC) simulations confirm this interpretation of the data. These simulations further allow for a measurement of the torque acting on the braids and an estimate of their effective torsional modulus. We show that the braiding of two molecules is well described by a simple geometric model: a twisted swing. The diameter of the DNA braid, which results from both entropic and electrostatic repulsive interactions, can be deduced by fitting this model to the experimental data. The variation of the braids' diameter with increasing force (which reduces entropic effects) and ionic strength can thus be investigated. The effective torsional modulus of the braids deduced from this simple model

Submitted November 30, 2004, and accepted for publication March 14, 2005.
Address reprint requests to Gilles Charvin, Tel.: 33-1-443-2-3492; E-mail: gilles.charvin@lps.ens.fr.

0006-3495/05/06/4124/13 $2.00
doi: 10.1529/biophysj.104.056945

agrees with the numerical (MC) estimates. Finally, we suggest that the sharp hysteretic transition observed (Strick et al., 1998) at low salt results from the melting of the two nicked DNA molecules, leading to the intertwining of stretched single strands.

MATERIALS AND METHODS

DNA constructs and micromanipulation setup

We labeled an 11-kb nicked DNA (linking number $Lk_0 \simeq 1100$) at its extremities with biotin and digoxygenin (DIG), as previously described in Strick et al. (1998). Nicks in the DNA molecules occur randomly during the various molecular biology steps of the synthesis. Their number as well as their position is not controlled, although it is not likely that this number exceeds 10 per molecule, or that the DNA presents large single-strand gaps. The molecules were bound at one end to a streptavidin-coated, 2.8 μm magnetic Dynal bead (Dynal Biotech, Lake Success, NY) and at the other to an anti-DIG-coated glass surface, previously incubated with BSA (Roche, Nutley, NJ) to reduce nonspecific interactions.

To stretch and braid the molecules, we used small magnets placed above the sample that can be displaced to set the force pulling on the molecules and rotated to braid them. Bead tracking and force measurement were performed on an inverted microscope (Strick et al., 1996). The extension z is measured by tracking the three-dimensional position of the tethered bead (Strick et al., 1998), with an error due to Brownian motion of ~10 nm (with 1-s averaging).

The bead's transverse fluctuations $\langle \delta x^2 \rangle$ allow for a determination of the stretching force using the equipartition theorem $F = k_B T z / \langle \delta x^2 \rangle$, where k_B is the Boltzmann constant and T the temperature (at 25°C, $k_B T = 4$ pN nm). Here F was measured with 10% accuracy.

In plots showing the recording of the DNA's extension, the points correspond to the raw data and were obtained at 25 Hz. For the curve-displaying extension versus catenation number n, each point was averaged over 256 frames. To eliminate microscope drifts, differential tracking with a second bead glued to the surface was performed.

Geometric model

Simple geometric considerations allow for a description of the braiding of two DNA molecules. We assume that the DNA molecules of length z_0 form a helix, whose diameter D does not vary with the braiding number n.

Calculation of the extension z versus catenation number n

The regime before contact ($|n| < 1/2$). Let us define by $z_0 \equiv z(n = 0)$ the extension of the molecules at $n = 0$. The variation of the extension $z(n)$ with the first half-turn (i.e., until the ''ropes'' are in contact) obeys

$$z(n) = \sqrt{z_0^2 - 4e^2 \sin^2 \pi |n|}. \quad (1)$$

The regime of braiding ($1/2 < |n| < n_c$). As the molecules are twisted beyond $n = 1/2$, we assume that their braiding results in the formation of a helical structure of fixed diameter D and braid angle α (Fig. 1), which is constant all along the molecules, but varies as n changes. A simple trigonometric argument (see Fig. 1), yields the extension $z(n)$:

$$z(n) = z_0 \cos \alpha = \sqrt{z_0^2 - (2e + \pi D(|n| - 1/2))^2}. \quad (2)$$

Notice that the larger n, the larger α. This is in contrast with the structure of a supercoil, for which the angle of the super-helix is constant when at $\sigma > 0.03$ (Vologodskii and Cozzarelli, 1996). Beyond a certain number of turns

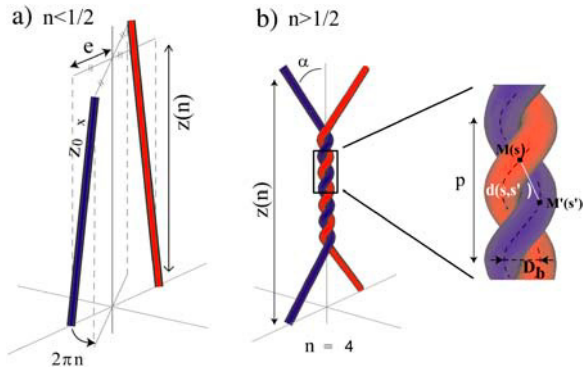

FIGURE 1 Geometric model for DNA braiding. (*a*) The case $|n| < 0.5$, where simple geometric considerations allow one to derive the extension $z(n)$ as a function of the angle $2\pi n$, the length $z_0 = z(n = 0)$, and the distance $2e$ between the molecules of $z(n) = \sqrt{z_0^2 - 4e^2 \sin^2 \pi |n|}$. (*b*) The case $|n| > 0.5$, where further braiding leads to the formation of a helix with diameter D_b, so that the extension $z(n)$ follows $z(n) = z_0 \cos \alpha = \sqrt{z_0^2 - (2e + \pi D_b(|n| - 1/2))^2}$. This model remains valid as long as the molecules are not in close contact, a condition reached when $d(s, s') \equiv \|\vec{M} M'(s, s')\| = D_b$, i.e., when the braid angle α reaches $\alpha_c = 45°$ (see Materials and Methods for details).

n_c, the molecule get into close contact, so that the geometric model is no longer valid. This is described in the next paragraph.

Close contact condition

Two molecules in the braid are not in close contact as long as the distance $d(s, s')$ between any two points $M(s)$ and $M'(s')$ on the molecules' axes is larger than D (where s, s' label the curvilinear coordinates along the molecules' axes; see Neukirch and van der Heidjen, 2002, for in-depth considerations about the geometry of braids). See Fig. 1 for

$$M(s) = \begin{pmatrix} D \sin(2\pi s)/2 \\ D \cos(2\pi s)/2 \\ ps \end{pmatrix}$$

and

$$M'(s') = \begin{pmatrix} D \sin(2\pi s' + \pi)/2 \\ D \cos(2\pi s' + \pi)/2 \\ ps' \end{pmatrix},$$

where $p = \pi D/\tan \alpha$ is the braid pitch. The condition $d(s, s') > D$ ($\forall (s, s')$) remains valid as long as

$$\frac{d^2(s, s')}{D^2} - 1 = \left[\left(\frac{\pi(s - s')}{\tan \alpha} \right)^2 - \sin^2 \pi(s - s') \right] \geq 0,$$

which implies $\tan \alpha \leq 1$, i.e., $\alpha \leq \alpha_c = 45°$.

Torque Γ as a function of n

The work W_t performed while twisting the two molecules is equal to the work done against the force $W = F(z_0 - z(n))$ plus the bending energy of the braid, $E_b = \xi L_{braided}(n)/2\mathcal{R}^2$, where $\mathcal{R}$ is the braid effective radius of curvature and $L_{braided}(n)$ is the length of braided DNA . The torque $\Gamma(n)$ stored in the braid is deduced from

$$\Gamma(n) = -\frac{1}{2\pi} \frac{\partial W_t}{\partial n}. \quad (3)$$

When $n < 1/2$, there is no bending energy, so that Eq. 3 yields

$$\Gamma(n) = \frac{\partial W}{\partial n} = \frac{2e^2\pi \sin(2\pi n)}{z(n)}. \quad (4)$$

As the chains are braided for $n > 1/2$, $\Gamma(n)$ becomes

$$\Gamma(n) = \frac{FD \tan \alpha}{2} \quad (5)$$

$$+ \frac{\xi}{Dz_0}\sin^2 \alpha(z_0 \sin \alpha + 3\pi D(n - 1/2)), \quad (6)$$

with $\sin \alpha = (2e+\pi D(n - 1/2))/z_0$.

Monte Carlo calculations

DNA modeling

The two DNAs were modeled as discrete worm-like chains (WLCs) constituted by $N = 120$ rigid segments of fixed length ($a = 10$ nm), so that the chain length was $L_0 = 1.2\ \mu$m. If θ_i is the angle between adjacent segments $i,i + 1$, the bending energy E_b associated to a given chain configuration is

$$E_b = \alpha k_B T \sum_{i=1}^{N-1} \theta_i^2$$

(Frank-Kamenetskii et al., 1985), where k_B is the Boltzmann constant, T the temperature, and $\alpha = 2.409$ the bending rigidity constant. The value α is set so that the persistence length of the chain corresponds indeed to five rigid segments (Frank-Kamenetskii et al., 1985), a discretization which has been shown to provide an accurate simulation of a DNA molecule (Vologodskii and Frank-Kamenetskii, 1992). Because of the application of a force F in the z direction, each segment tends to align along the force, which results in an additional energy term $E_F = -Fz$, where z is the extension of the braid.

Monte Carlo procedure

A Metropolis Monte Carlo algorithm (Metropolis et al., 1953) was used to generate a set of conformations that satisfy the equilibrium, as described in Klenin et al. (1991). We randomly applied moves (described in the next paragraph) to a given braid configuration c (of energy E) to generate a new trial configuration c'. We calculated the new energy of the braid E', and accepted the new configuration with probability $P = min\{1, \exp(-(E' - E)/k_BT)\}$. This process was then iterated N_{MC} times. A large number of iterations were required to get a reliable estimate of the braid's configuration; see below.

Moves

Two types of moves were used to generate new trial configurations: first, we chose a segment i and changed its angle ϕ_i with the z axis to an arbitrary value (uniformly distributed in $\cos(\phi_i) \in [-1, 1]$), while keeping the orientation of all other segments fixed. Second, we randomly chose two vertices i and j in one chain and rotated all the segments between these two vertices by an angle ϵ around the axis Δ_{ij} passing through the vertices. The value of ϵ was randomly chosen in an interval $[-\epsilon_{max}; \epsilon_{max}]$. The value ϵ_{max} was set so that the rate of acceptance was 25%. Note that this move did not change the extension of the chain.

Additional energy term to keep the relative position of the anchoring points

Although the spacing between the chains was kept fixed at the bottom of the braids, we had to allow small variations of the spacing and orientation at their top, to allow for changes in the chains' conformation. This was achieved by adding three potential energy terms, namely E_o, E_d, and E_t, to the total energy of the chain. If $\vec{\tau}_1$ ($= 2e\hat{x}$) and $\vec{\tau}_2$ are the vector joining the anchoring points, respectively, at the bottom and the top of the braid, and β the angle between $\vec{\tau}_1$ and $\vec{\tau}_2$, these terms are

$$E_o = \frac{1}{2}k_o(\vec{\tau}_2.\hat{z})^2$$

$$E_d = \frac{1}{2}k_d(\|\vec{\tau}_2\| - 2e)^2$$

$$E_t = \frac{1}{2}k_t\beta^2$$

The value E_o ensures that $\vec{\tau}_2$ is orthogonal to the direction of the force, $\hat{z}$. The value E_d prevents the spacing between the molecules from deviating too much from its average value $2e$. The value E_t limits the angular fluctuations of β. Measuring the mean deviation $\langle\beta\rangle$ allows for an estimation of the torque in the braid.

Topological constraints

Because of the moves occurring during the Metropolis procedure, the linking number n between the two chains may change. We selected the conformations that had the right linking between chains by calculating the Alexander polynomials for two linked chains (Frank-Kamenetskii and Vologodskii, 1981). Configurations with the wrong linking number were rejected. We also used Alexander polynomials to evaluate the knotting in the chain formed by the closing of the two subchains (Frank-Kamenetskii and Vologodskii, 1981) and rejected all conformations with the wrong topology.

Excluded volume effect and electrostatic interactions

We took into account the excluded volume and electrostatic interactions by introducing a hardcore diameter D_{DNA} for each segment (Stigter, 1977; Rybenkov et al., 1993). We discarded configurations whose segments were intersecting each other.

Measurements of correlations in the Monte Carlo process

To estimate the number N_C of Monte Carlo (MC) steps necessary to obtain decorrelated configurations, we used a method based on the calculation of the error in the extension mean, as described in depth in Flyvbjerg and Petersen (1989).

The method relies on the following idea: if the extension z is a random variable with a mean value z_0 and a standard deviation σ, these parameters can be estimated by using the simple formula $z_0 = \langle z_i\rangle$ and $\sigma = \langle(z_i - z_0)^2\rangle^{1/2}$, where z_i is the extension of the configuration of index i. These equalities are mathematically valid only if two hypotheses are fulfilled: the averaging is done on a large number of samples N, and these samples are uncorrelated. Of course, those two conditions are seldom fulfilled. The number of samples N is always finite, which leads to an error in the estimation of z_{0N} and σ_N; their relative accuracy will typically scale like $N^{-1/2}$, the error on z_{0N} being equal to $\sigma_N/N^{-1/2}$. These results are a consequence of the so-called central-limit theorem.

The correlations between successive z_i effects have a more serious impact: their effects are to reduce the fluctuations of successive z_i, leading to an underestimation of the error on z_{0N} computed by $\sigma_N/N^{-1/2}$. A way to evaluate the correlation is simply to try and check the validity of the central-limit theorem. By using a long series of z_i, we build a series of data $z_j^{N_b}$ corresponding to the average of z_i over N_b consecutive points ($N_b = N \times Q$ all integer) with i between $N_b \times j$ and $N_b \times (j + 1)$. We then compute σ^{N_b} and evaluate the error in z_0 as $\sigma_{z_0}^{N_b} = \sigma^{N_b}/(N/N_b)^{-1/2}$ and repeat this process while increasing N_b. Two situations occur. If N_b is large enough that the

correlation between z_i and z_{i+N_b} has disappeared, the central-limit theorem applies, and $\sigma_{z_0}^{N_b}$ is independent of N_b. However, if N_b is too small, the correlation reduces the fluctuations and $\sigma_{z_0}^{N_b}$ decreases while decreasing N_b. The transition between these two regimes occurs at a value N_C corresponding to the correlation size of the series. Of course N has to be much larger than N_C, otherwise $\sigma_{z_0}^{N_b}$ is continuously increasing with N_b and never reaches its asymptotic value. Typically N needs to be 100 times larger than N_C. The ratio N/N_C gives the number of uncorrelated points in the data series.

According to this method, we iteratively computed the error in $z_0 \equiv \langle z \rangle$ with bins of growing size N_b (corresponding to 10,000 N_b MC steps), as shown in Fig. 2 *a* (for the case of $n = 6$ braids). We obtained an estimate of the number of correlated MC steps N_C ($N_C = 660{,}000$ for $n = 2$). N_C appears to vary exponentially with the number of braids n (see Fig. 2 *b*): $N_C = A \exp(Bn)$, where $A = 44{,}000$ and $B = 0.46$, thus indicating that braiding the chains restricts the ability of the MC algorithm to effectively explore the phase space and to rapidly reach thermodynamic equilibrium. Consequently, to ensure a statistically relevant ensemble of independently relaxed configurations we set the total number of MC steps as $N > 100\, N_C$.

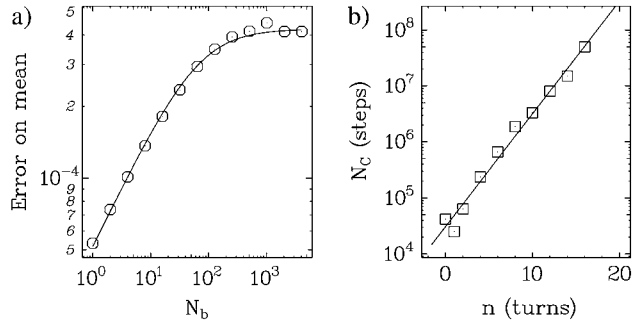

FIGURE 2 Measurements of correlation in the generation of Monte Carlo configurations. (*a*) Open circle is the error on mean (δ) as a function of bin-size N_b (see text for details) obtained at $n = 6$ (with $2e/L_0 = 0.36$ and $D_{DNA} = 6$ nm). Solid line is the curve obtained by fitting the numerical data to $\delta(N_b) = \delta_0/\sqrt{1 + N_C/(10{,}000\, N_b)}$. N_C yields an estimate of the number of correlated steps. In the case where $n = 6$, we obtained $N_C = 660{,}000$. (*b*) Open square is the variation of N_C with the number of applied turns n, and exponential fit as $N_C = A \exp(Bn)$, with $A = 23{,}000$ and $B = 0.47$. The higher the braiding number, the larger the number of MC configurations required to characterize the chain.

EXPERIMENTAL RESULTS

Force versus extension curves for two unbraided molecules

To study the braiding of two DNA molecules, we have anchored two nicked 11-kb DNA molecules (crystallographic length $L_0 = 3.6\ \mu$m) on the same superparamagnetic bead (Strick et al., 1998). This was achieved by incubating streptavidin-coated magnetic beads (Dynal) with biotin end-labeled DNA at an appropriate DNA/bead ratio. The DNA/bead construct was injected in an anti-DIG-coated square capillary tube, to which surface the molecules could bind via their second extremity labeled with DIG (see Fig. 3).

The DNA/bead ratio was set such that the probability of anchoring by many molecules was much lower than the probability of tethering by a single DNA. This ensures that the few beads anchored by two molecules are much more frequent than beads anchored by three or more molecules. A force is applied on the bead by using the magnetic trap setup, as described by Strick et al. (1998). This setup allows one to rotate the magnets and thus to braid the two molecules tethering the bead to the surface. Such doubly anchored beads can be discriminated easily from beads anchored by a single DNA molecule. Since the molecules are nicked, singly anchored beads are insensitive to rotation of the magnets, whereas multipally anchored beads recoil to the surface as a result of braiding.

We applied a magnetic force on the bead F by creating a magnetic field gradient using small magnets in the vicinity of the glass capillary. This force can be varied by changing the distance between the magnets and the sample. Once multipally anchored beads have been identified, we checked that they were bound by two DNA molecules by measuring the force-extension response of the system and comparing it to the WLC model. We hypothesized that there were two molecules bound in parallel to the bead, so that the force F_{1mol} felt by each molecule would be half the stretching force F. Thus, plotting F_{1mol} as a function of extension should agree with the WLC and should output the persistence length expected for DNA in these conditions. Fig. 4 shows the force extension curves obtained with one tethering (in this case, $F_{1mol} = F$) and two tethering DNA molecules ($F_{1mol} = F/2$), respectively. The best fit to the WLC yields $\xi = 46 \pm 5$ nm and $\xi = 44 \pm 4$ nm, respectively, thus validating that our bead was doubly anchored in the latter case. A lower persistent length in the latter case would have been found in the case of three or more tethering molecules.

Notice that, in principle, the distance between the anchoring points on the beads and the surface need not be

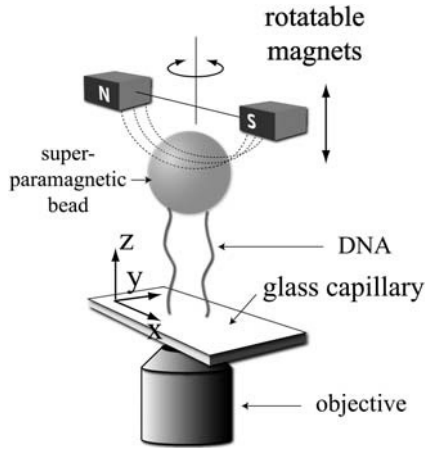

FIGURE 3 Sketch of the experimental setup. Two DNA molecules are multipally tagged at their extremities with biotin and digoxygenin (DIG), so that they can be attached to a streptavidin-coated superparamagnetic bead and to an anti-DIG-coated glass surface. Translation and rotation of small magnets close to the DNA molecules by a few-mm change of the applied force and the number of braids, respectively. The DNA molecule's extension is measured by tracking the position of the bead using an inverted microscope (see Materials and Methods for details).

the same, and indeed, constitutes the large majority of sets of molecules we found in the capillary after injection of the DNA-bead mix. When the molecules are stretched in such a trapezoidal conformation, the distance of the bead to the surface $z(F)$ will be smaller than one single molecule's extension at one-half the force $L(F/2)$. Such beads are not considered in the following, where we focus our attention on those constructs for which $z(F) \approx L(F/2)$.

Extension $z(n)$ versus catenation number, n

By rotating the magnets above the sample, we are able to braid the molecules by n turns and to monitor the consecutive variations in their extension $z(n)$ (see Fig. 5). Three different regimes can be discerned (see *dashed lines* in Fig. 5):

1. $|n| \leq 1/2$. The first half-turn leads to a big decrease in the DNA's extension, which corresponds to the formation of a crossing between the two DNA. This large decrease is due to the fact that the distance between the molecules' anchoring points is comparable to the length of the molecules. Previous experiments on braided DNA did not report such an effect because the DNA used was longer (48 kb, Strick et al., 1998; and 41 kb, Stone et al., 2003). From the variation of extension between $n = 0$ and $n = 0.5$, we can calculate the spacing between the two molecules (see Materials and Methods). Note that this spacing is limited by the size of the bead, i.e., 2.8 μm.

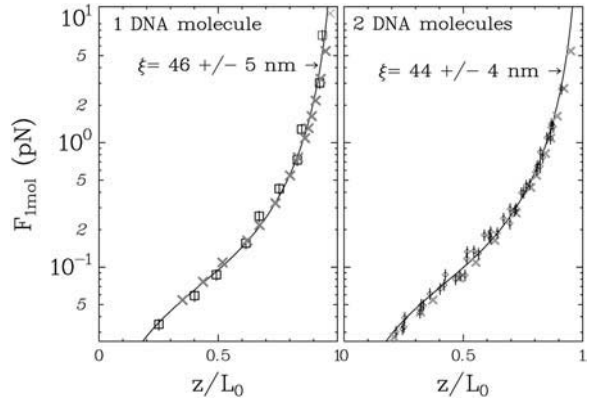

FIGURE 4 Force versus extension curve for one (*left plot*) and two (*right plot*) DNA molecules tethered to the same bead. The value F_{1mol} is the actual force felt by one molecule, i.e., $F_{1mol} = F$ in case of one tethering molecule, and $F_{1mol} = F/2$ in case of two molecules, where F is the stretching force. Open squares are the experimental points obtained with a single DNA molecule. Error bars indicate statistical error. The best fit (*solid line*) to the worm-like chain (WLC) model yields a persistence length $\xi = 46 \pm 5$ nm. Open diamonds are the experimental points obtained on different sets of two DNA molecules; the fit (*solid line*) using the WLC model yields $\xi = 44 \pm 4$ nm. Shaded crosses are the results obtained using a Monte Carlo simulation of the stretching of one (*left plot*) or two (*right plot*) unbraided molecules of persistence length 46 nm, according to the procedure described in Materials and Methods. Statistical errors of simulated curves are smaller than the size of the symbols. Small deviations from the WLC model at forces >2 pN are due to chain discretization (Vologodskii, 1994).

2. $1/2 < |n| < n_c$. Further rotation of the magnets leads to a smaller decrease in the system's extension per added turn. This regime corresponds to the formation of the braids. As we shall see below, the extension of the molecules in this domain is well described by the simple geometric model of a twisted swing.
3. $|n| > n_c$. At a critical number of turns n_c, the molecules get in close contact, so that the torque rapidly builds up and further rotation of the magnets leads to a buckling of the braids (Marko, 1997). That transition to a different regime of braiding is manifested by a change in the slope of the extension versus n plot. That transition is characterized by an increase in the fluctuations in extension, which is also observed in MC simulations of braided molecules.

Transition to plectonemes of braids and longitudinal fluctuations

To get a better understanding of the $n > n_c$ regime, we have monitored the longitudinal fluctuations of the system as a function of the catenation density, $Ca = n/Lk_0$, defined in the same manner as the supercoiling density ($\sigma = \Delta Lk/Lk_0$). This definition allows for a comparison between molecules of different size. Fig. 6 *a*) displays the extension measured for one set of molecules as a function of $Ca > 0$ (*shaded diamond*, right-handed braids) and $Ca < 0$ (*open diamond*, left-handed braids). Interestingly, we observe a small but consistent difference in the molecules' extension in the $Ca > 0$ versus the $Ca < 0$ regime, which suggests that right-handed braids are more stable than braids of opposite handedness: they can be twisted to a larger extent before they buckle. This phenomenon, which is observed only at high salt, could be due to the fact that the wrapping of two DNA molecules in a braid with the same chirality as DNA (right-handed) can lead to a more compact structure, thus decreasing the torque stored in the braid.

Fig. 6 *b* shows the averaged squared fluctuations in extension $\langle \delta z^2 \rangle$ normalized by the molecule's radius of gyration: $R_g^2 = \xi L_0/3$. Notice the large increase in noise when $Ca > 0.05$, which is correlated to a change in the slope of the extension versus rotation curve. This behavior indicates that the system's stiffness decreases at the buckling transition, consistent with the formation of plectonemes of braids (similar behavior is observed when stretched twisted DNA buckles to form supercoils; see Charvin et al., 2004).

MONTE CARLO SIMULATIONS

Force versus extension curves for two unbraided chains

To simulate the experimental data, we have performed Monte Carlo simulations (Vologodskii and Marko, 1997) of the braiding of two discrete WLCs of persistence length $\xi =$

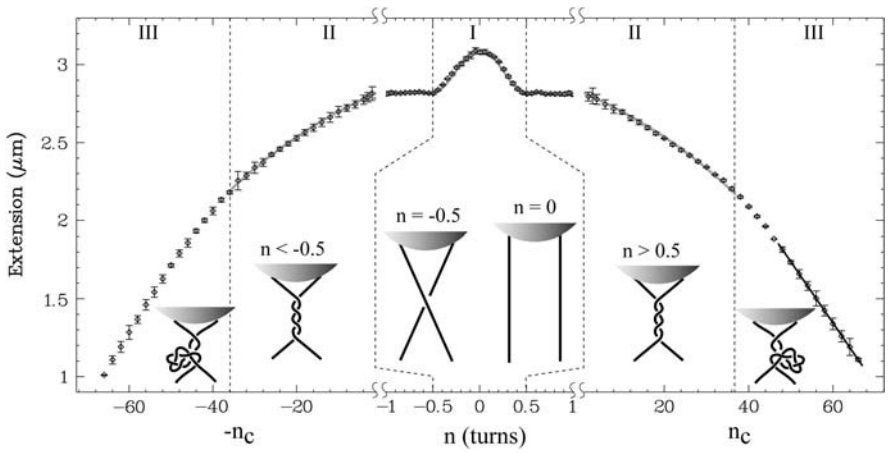

FIGURE 5 Extension versus braiding for two DNA molecules and sketches of the expected geometry of the braid. The open diamonds are experimental points, obtained at $F = 2$ pN in 100 mM PB. We distinguish three regimes of braiding, based on the geometrical model described in the text: (*I*) the regime $|n| < 0.5$, characterized by a sharp variation with n of the extension, before the crossing of the two molecules; (*II*) the regime $|n| > 0.5$, where the molecules are intertwined; and (*III*) the regime $|n| > n_c$, where the braids buckle and form plectonemes (supercoils of braids). Error bars indicate the statistical errors. A fit of the experimental data to the geometric model (in regimes *I* and *II*) yield the intermolecular spacing of $2e = 1.28 \pm 0.02$ μm and braids' diameter of $D_b = 8.2 \pm 0.2$ nm (*shaded line*). The line in regime *III* is a linear fit to the data in the plectonemic regime. The schematics represent the expected geometry of the braid in the different regimes.

46 nm (a faithful description of the elastic behavior of DNA; see Vologodskii and Frank-Kamenetskii, 1992; Vologodskii, 1994). Each molecule was modeled as a $L_0 = 1.2$ μm chain consisting of $N = 120$ rigid segments of 10-nm length each. This discretization of the molecule (five segments per persistence length) provides a good enough approximation of its entropic behavior at low forces $F < 10$ pN. The conformations of DNA molecules were generated using a Monte Carlo Metropolis algorithm (Metropolis et al., 1953), as described in Materials and Methods. The configurational space was randomly sampled by appropriate moves of the chain. The energy of the sampled configurations consisted of two terms: First, a bending energy proportional to the square of the angle (θ_i) between adjacent segments (i, $i + 1$) and calculated by summing over $i = 1, \ldots, N$; and second, a potential energy term resulting from the application of the force ($\vec{F}$), which tends to align all the segments in its direction (defined as the z axis). A new configuration was accepted with probability $P = 1$ if it lowered the energy of the chain and rejected with an appropriate probability $P < 1$ (see Materials and Methods) if it increased it. To check our algorithm we verified that the simulation of the pulling of two unlinked chains reproduced the expected elastic behavior of two WLC in parallel. Shaded symbols in Fig. 4 shows a force-extension curve obtained using a numerical simulation with one chain or two unlinked chains. The excellent agreement between these numerical data and the WLC predictions demonstrates the accuracy of our algorithm as a model of the elastic behavior of two DNA molecules.

When the chains are braided, the number of links n between the two chains must be kept constant during the simulation. However, as the moves used to generate new configurations may modify n, we used Alexander polynomials to assess the linking number and reject moves that altered it (Vologodskii et al., 1975). We applied the same method to reject knotted chains, although it was not necessary to perform this check at every move.

A reliable sampling of configuration space requires the generation of a large number of uncorrelated configurations (the method used to assess the MC correlation length was described in Materials and Methods). We typically generated between $N = 10^8$ and 4.10^9 (mostly correlated) configurations, which takes a lot of computer time, especially at large n (see Fig. 2 in Materials and Methods). As a consequence, we decided to focus on a comparison between simulation and experimental data for a given separation $2e$ between the molecules and DNA's effective diameter D_{DNA}, set by the ionic conditions of the experiment (Stigter, 1977).

Extension $z(n)$ versus catenation number n

The extension versus n curves for braided chains greatly depends on the spacing between the chains. To simulate the experimental data, we set the spacing $2e$ between the chains such that the ratio $2_e/L_0 \simeq 0.36$ was the same in the simulation as in the particular experiment shown in Fig. 5. The electrostatic repulsion between the DNA molecules sets its effective diameter, which in a solution containing 100 mM of monovalent salts has been calculated and measured to be $D_{DNA} = 6$ nm (Stigter, 1977; Rybenkov et al., 1993, 1997). To take that repulsion into account we have treated the chain's segments as hardcore cylinders of a diameter D_{DNA}. As shown in Fig. 7 *a*, a comparison between the simulated and the experimental data displays a good agreement over the whole range of catenation densities Ca investigated. Notice that the extension is sensitive to the value of D_{DNA}: simulations with $D_{DNA} = 5$ nm (corresponding to 200 mM monovalent salt) or 4.2 nm (in 100 mM PB + 5 mM Mg^{2+}) do not provide as good a fit to the data. However, for $Ca >$

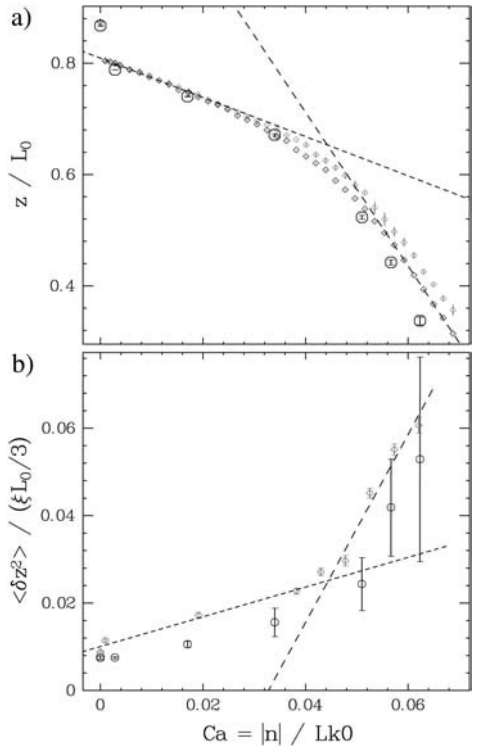

FIGURE 6 Experimental and numerical characterization of the braids' plectonemic regime. (*a*) Normalized extension (z/L_0 where $L_0 = 3.56$ μm is the molecules' length) versus catenation density $Ca = |n|/Lk_0$ for $n > 0$ (*shaded diamonds*) and $n < 0$ (*open diamonds*; $F = 2$ pN in 100 mM PB + 5 mM $MgCl_2$). Error bars indicate the statistical error. Notice the slight difference between left-handed (*L*; negative, $n < 0$) and right-handed (*R*; positive, $n > 0$) braids at high catenation density. This difference reflects the right-handed chirality of the DNA molecules, which can be positively braided to a larger extent before buckling than negative (left-handed) braids. Open circles are the numerical simulations of the braiding of two WLC polymers of extension $L_0 = 1.2$ μm, intermolecular distance $2e/L_0 = 0.36$, and effective diameter $D_{DNA} = 4.2$ nm, determined from the ionic conditions of the experiments (Rybenkov et al., 1997). (*Dashed lines* mark the differences in slope between the two regimes of braiding.) (*b*) Averaged normalized fluctuations in the braid's extension $\langle \delta z^2 \rangle / (\xi L_0/3)$ as a function of *Ca* for the experimental (*shaded diamonds*, $n > 0$) and the simulated (*open circles*) runs shown in *a*. The fluctuations increase for $Ca > 0.05$, i.e., the system becomes more flexible as expected from the formation of supercoils of braids. The dashed lines mark the differences between the two regimes of braiding. Notice that the error bars in the estimate of the fluctuations in extension (from MC simulations) are larger than in the estimate of the mean extension. The dashed lines in both *a* and *b* cross at the same value of *Ca*, which indicates that the transition to supercoils of braids is associated with both a structural change (formation of plectonemes) and a decrease in stiffness (increase in fluctuations).

0.04 the simulation with a smaller effective radius ($D_{DNA} =$ 5 nm) seems to fit the experimental data slightly better. It should be noted that the concept of the DNA effective diameter assumes equal probability of all mutual orientation interacting segments (Vologodskii and Cozzarelli, 1995). The assumption is not valid for tight DNA braids, and therefore accounting for the electrostatic repulsion in terms of DNA effective diameter is less accurate in this case. It is also possible that the increased torque in the braids at high catenation number forces the molecules in closer contact, reducing the value of D_{DNA} estimated from pure electrostatic repulsion. This is consistent with the observation, at high catenation number, of slightly different extensions for right- or left-handed braided DNA. Notice finally the transition in the simulations to plectonemes of braids at $Ca_c \sim 0.04$–0.05.

Good agreement between the simulations and the experimental data is also obtained for different ionic conditions (100 mM PB + 5 mM Mg^+ + for which $D_{DNA} = 4.2$ nm; Vologodskii and Marko, 1997); see Fig. 6 *a*. Moreover, the fluctuations in extension for both the experimental and simulated data are similar and exhibit, as expected (see Experimental Results), a larger increase in their amplitude in the regime of plectonemes of braids. The slightly larger amplitude of fluctuations in the experiment is probably due to various external sources of noise, absent from the simulations.

Our simulations therefore provide an excellent description of the braiding of two DNA molecules. However, whereas in the experiments we have no control on the distance between the two braided molecules, in the simulations this is an adjustable parameter. We can therefore simulate the intertwining of the daughter strands during replication as they are joined at the replication forks, much more easily than we can reproduce that configuration experimentally (that would require a special construct which we have not attempted). The results of that simulation are shown in Fig. 7 *b*. At low catenation number one notices that the braids are localized near the anchoring points, a configuration that maximizes the entropy in the rest of the chain (Marko, 1997). This localization of the topological constraint seems to be a general feature of random chains also reported for knotted or catenated plasmids. It has been invoked to explain the amazing property of the type II topoisomerases, which, despite acting locally on DNA crossings, are capable of reducing their topological entanglement (a global property of the chain(s)) (Marko, 1997; Vologodskii et al., 2001). In the present instance our simulations suggest that the links between the replicated daughter strands (and therefore probably the topoisomerases) will be localized near the replication fork.

At high catenation number, the intertwined daughter strands undergo a buckling transition to plectonemes of braids. That transition is observed at $Ca_{c,0} \sim 0.075$, which is higher than the value $Ca_c \sim 0.05$ estimated for molecules anchored a relative distance $2e/L_0 = 0.36$ from each other. However, in that case, the effective length of braided DNA is ~36% smaller. Normalizing the number of braids by the length of the DNA actually being braided yields a value of $Ca'_c \sim 0.078$, close to the value estimated for intertwined daughter strands.

Force versus *Ca* phase diagram

In bacteria, the catenation density *Ca* during the replication process is difficult to evaluate, since it results from a balance

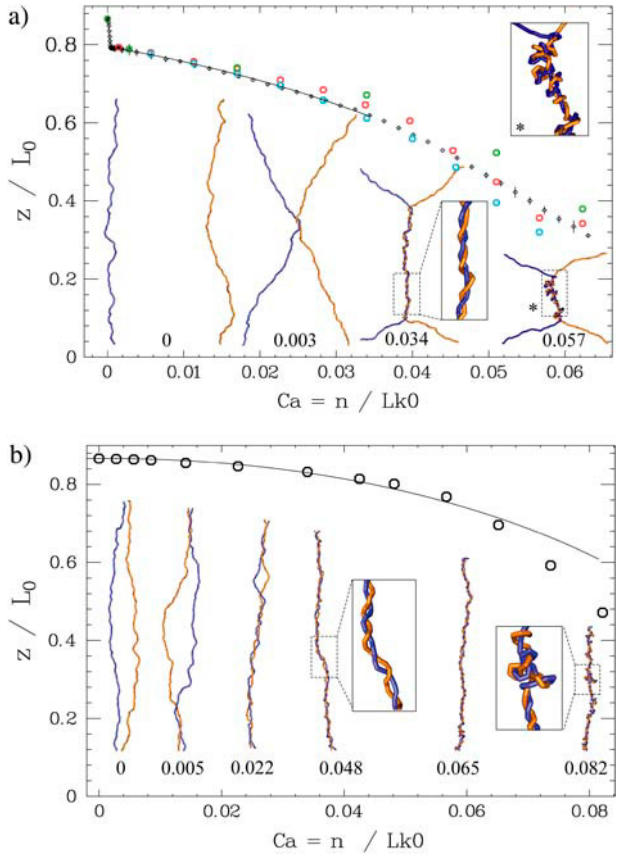

FIGURE 7 Relative extension z/L_0 versus catenation density Ca in numerical simulation of the braiding of two polymer chains and comparison with the experimental data in 100 mM PB (same molecule as in Fig. 8 but in different ionic conditions). (*a*) Normalized extension as a function of Ca obtained in an MC simulation of two chains of extension $L_0 = 1.2$ μm, intermolecular distance $2e/L_0 = 0.36$ at $F = 2$ pN using an effective DNA diameter $D_{DNA} = 6$ nm (*blue circles*, corresponding to the experimental ionic conditions), $D_{DNA} = 5$ nm (*red circles*), and $D_{DNA} = 4.2$ nm (*green circles*). The open diamonds are experimental data. The solid line is a fit of the numerical data to the geometric model (described in the text) with a braid's diameter $D_b = 8.8$ nm $> D_{DNA} = 6$ nm due to entropic repulsion. The errors bars in the estimates of the simulated extension are smaller than the size of the symbols. (*b*) Numerical results obtained using $2e/L_0 = 0.02$ (*open circles*). The solid line is a fit of the numerical data to the geometric model with $D_b = 7.4$ nm. The schematics display some typical braid configurations obtained at various Ca values indicated below each structure. Note that all these simulations were done with $Ca > 0$ (the braid helix is right-handed), but identical results were obtained with $Ca < 0$, since we do not take DNA chirality in the simulation into account.

between the rate of progression of the replication complex and the rate of supercoils and pre-catenanes removal by Type II topoisomerases. Recently, it has been shown that the bacterial type II topoisomerase, Topo IV, efficiently unlinks right-handed braided DNA molecules only when they form plectonemes (Charvin et al., 2003; Stone et al., 2003). It is thus interesting to get an estimation of the range of forces and catenation density, Ca, which lead to the formation of supercoils of braids. To that purpose, we have performed numerical simulations of braided daughter strands ($e = 0$) at different forces and braiding densities. Based on the analysis of the braids' structures, we plot in Fig. 8 the phase diagram for buckled and unbuckled DNA catenanes. This plot reveals that the critical force for buckling increases with the braiding number Ca faster than exponentially.

The supercoiling induced tension in a typical plasmid with $\sigma = -0.06$ is $F \approx 0.6$ pN (Charvin et al., 2004). In such a plasmid one can estimate from Fig. 8 that buckling of the replicated daughter strands will occur at a catenation density of $Ca \sim 0.065$. Previous studies of replication intermediates (Adams et al., 1992) suggest that their catenation density is $Ca \sim 0.01$, meaning that plectonemes of catenanes are either not generated during replication, or are transiently localized near the replication fork and relaxed by the action of topoisomerases.

Numerical estimation of the braid's torsional modulus

The determination of the value of the torsional modulus of double-stranded DNA is still a subject of controversy, with values ranging from $C = 50$ nm k_BT and $C = 120$ nm k_BT depending on ionic conditions (Neukirch, 2004) and the method used (Charvin et al., 2004). A related question is to determine the torsional persistence length of a DNA braid composed of two nicked double-stranded DNAs. In contrast with the torsional modulus of DNA, which depends upon its intrinsic material properties, the effective torsional modulus of braided chains is of entropic origin and can thus be deduced from MC simulations. Due to the large torsional stiffness of the magnetic trap it was unfortunately not possible to compare these numerical results to a measurement of the torsional modulus of DNA braids.

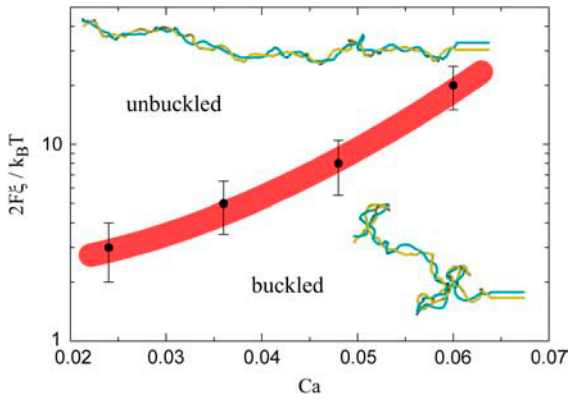

FIGURE 8 Force versus Ca ($Ca > 0$) phase diagram for the buckling of braids (with $2e/L_0 \ll 1$). The MC simulations of braids at various forces and catenation densities (Ca) allow us to determine the limit between buckled and unbuckled states. The black points display the position of the buckling transition at a given Ca. Error bars represent statistical error. The thick shaded line indicates the position of the buckling line. Typical conformations in each phase (buckled or unbuckled) are shown. The dimensionless unit used on the y axis involved the persistence length ξ of a single DNA molecule.

Let τ_1 and τ_2 be the vectors joining the anchoring points of the two chains at the bottom and the top of the braid, respectively (see Fig. 9 *a*). To compute the torque in the braids from the MC simulations, we do not impose $\tau_1 = \tau_2$, but let the angle $\beta(\ll\pi)$ between these two vectors vary slightly under the torque acting on the braids. To that purpose we introduce, in the energetics of the chains, an elastic energy term of $E_t = k_t\beta^2/2$ (see Materials and Methods), with $k_t = 2000\ k_BT/\text{rad}^2$ for $n < 1/2$ and $k_t = 200\ k_BT/\text{rad}^2$ for $n > 1/2$. From the MC simulations we can obtain an estimate of the average torque in a braided chain as $\langle\Gamma\rangle = k_t\ \langle\beta\rangle$, and from the variation of this torque with n, we can derive the torsional modulus of the braids as $C_b = (L_0/2\pi)\partial\langle\Gamma\rangle/\partial n$.

Fig. 9, *b* and *c*, displays the values of $\langle\Gamma\rangle$ obtained in the two regimes $n < 1/2$ and $n > 1/2$ for the simulation runs shown in Fig. 7. When $n < 1/2$, the large spacing between anchoring points ($2e/L_0 = 0.36$) introduces a large increase in the torque (*solid points*), which is maximal at $\sim n = 1/4$ ($\sim 25\ k_BT/rad$) and then decreases back to $\sim 2\ k_BT/rad$ at $n = 1/2$. This sharp variation in the torque is absent when the molecules are anchored at the same point (or very close to each other, data not shown).

When $n > 1/2$, the torque rises almost linearly with n, whether the spacing between anchoring points is large ($2e/L_0 = 0.36$, *solid points*) or very small ($2e/L_0 = 0.02$, *shaded points*). Interestingly, the torque does not seem to saturate past the buckling threshold, although more data are needed in this regime, which is hard to simulate. A linear fit to the numerical results allows us to deduce the braids' torsional modulus, $C_b/k_BT = 63 \pm 6$ nm at a large intermolecular distance ($2e/L_0 = 0.36$), and $C_b/k_BT = 48 \pm 1$ nm for chains anchored at the same point ($2e/L_0 \ll 1$). Surprisingly, C_b does not depend much on the spacing between the molecules. In fact, correcting the value of C_b estimated at $2e/L_0 = 0.36$ by the length of DNA effectively braided ($\sim 0.64\ L_0$) yields a value $C'_b \sim 41$ nm in even better agreement with the value at $2e/L_0 \ll 1$.

A GEOMETRICAL MODEL FOR DNA BRAIDING

Extension $z(n)$ versus catenation number n

To provide a phenomenological understanding of the behavior of braided DNA, we have proposed a model that describes the braiding of the molecules anchored a distance $2e$ from each other in analogy with the intertwining by n turns of the two ropes of a swing (see Fig. 1). This model is a refinement of a model previously proposed for the braiding of two molecules anchored at the same point ($2e = 0$) (Strick et al., 1998). The diameter D_b of the braid need not be equal to the crystallographic diameter of DNA, since entropic fluctuations and electrostatic repulsion between the two molecules will tend to increase the intermolecular distance between the two molecules. The elastic behavior of such a twisted swing is characterized by the two regimes $n < 1/2$ and $n > 1/2$, as described in Materials and Methods (see also Fig. 1).

When $n < 1/2$, there is no contact between molecules. There is an excellent agreement between the braid extension predicted by Eq. 1 (see Materials and Methods) and our data, which enables us to estimate the distance $2e$ between the molecules' anchoring points. For the particular data shown in Fig. 5, $e = 0.64 \pm 0.02\ \mu$m. The value z_0 is deduced directly from the value $z(n = 0)$ of the plot.

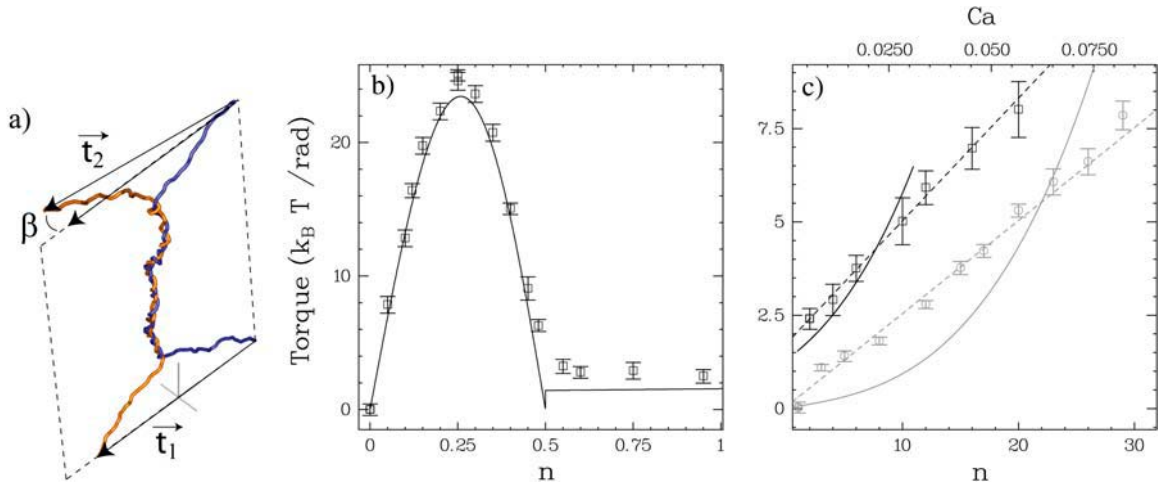

FIGURE 9 Determination of the torque in the braid. (*a*) Schematics: the torque is estimated by calculating the deviation angle β between the two vectors τ_1 and τ_2 between the anchoring points (see text for details). (*b*) Regime $n < 1/2$. The points display the values estimated from the simulations, whereas the solid line is the torque expected from the geometric model (when $2e/L_0 = 0.36$, with no fit parameter). (*c*) The regime $n > 1/2$. Results from numerical simulations at $2e/L_0$ (*solid squares*) and $2e/L_0 = 0.02$ (*shaded squares*) and comparison with the estimates from the geometric model (*solid* and *shaded curves*, respectively). Clearly the model fails to predict the variation of Γ with n, in particular when $2e/L_0 \ll 1$. Errors bars indicate statistical errors. (The *solid* and *shaded dashed lines* are linear fits to the numerical data from which we compute the torsional modulus of the braids, C_b, 63 ± 6 nm k_BT and 48 ± 1 nm k_BT, respectively.)

As the molecules are further braided they form a helical structure of fixed diameter D_b and varying braid angle α. The very good fit between the extension predicted by this geometric model (see Eq. 2 in Materials and Methods) and the data allows us to extract the diameter of the DNA braid D_b (for the data in Fig. 5, $D_b = 8.2 \pm 0.2$ nm). This value is larger than the crystallographic diameter of DNA (2 nm), but also larger than the effective diameter of DNA, $D_{DNA} = 6$ nm, which was used in the numerical simulations to fit the experimental data (see above). The reason for this discrepancy is that in the simple model considered here the larger diameter of the braids results not only from electrostatic repulsion but also from entropic contributions (which are naturally taken care of in the MC simulations). As we shall see below, the geometric model allows us to extract the respective contributions of these interactions at various forces and ionic strengths.

Eq. 2 remains valid as long as the molecules are not in close contact, i.e., when $\alpha \leq \alpha_c = 45°$ (see Materials and Methods for a proof of that point). Beyond that value, the torque in the braided molecules leads to their mechanical buckling, i.e., to the formation of the plectonemes of braids previously described (see Experimental Results, and Monte Carlo Simulations, above).

Braid diameter versus force and salt

We have experimentally investigated the influence of entropic and electrostatic repulsion interactions on the braid diameter D_b. We can modulate the strength of the entropic repulsion between the molecules by varying the stretching force: the larger the force, the smaller the fluctuations of the molecules; the smaller their entropic repulsion, the smaller D_b is. By changing the ionic conditions, we similarly modulate the electrostatic repulsion range (Debye length) between the molecules. The lower the ionic strength, the larger the Debye length, and the larger the D_b.

Fig. 10, *a* and *b*, display the variation of extension with the number of braids n obtained in different phosphate buffers and at different forces. Fitting the various curves to the geometric model previously introduced allow us to retrieve the braid diameter as a function of force and ionic strength (see Fig. 10 *c*). Increasing the tension reduces the entropic fluctuations and decreases the braid diameter. At any given salt conditions, the dependence of D_b on the force is well fit (see Fig. 10 *c*) by the prediction of Marko (1997), as

$$D_b = D_{b,\infty} + AF^{-3/4},$$

where $D_{b,\infty}$ is the braid diameter at very large forces, in which only electrostatic repulsion should play a role. As shown in Fig. 10, $D_{b,\infty}$ increases linearly with the Debye length λ_D (Zhang et al., 2001). Note that in 100 mM PB, $D_{b,\infty} = 5.6 \pm 0.3$ nm, close to the value of the effective diameter of DNA in these ionic conditions—which is $D_{DNA} = 6$ nm.

Estimating the torque in braided chains from the geometric model

The numerical estimates of the torque in braided chains can be understood within the framework of the simple geometric model previously described. Under the assumptions of this model, the work W_t performed while twisting the two DNA molecules by n turns is balanced by two terms: first, the work W done against the force pulling on the molecules and second, the bending energy of the braided DNA molecules. From the calculation of that energy (detailed in Materials and Methods), one can deduce the torque stored in the braid $\Gamma(n) = 1/(2\pi)\partial W_t/\partial n$.

When $n < 1/2$, there is no contact between molecules and no bending. The torque is due purely to the work against the

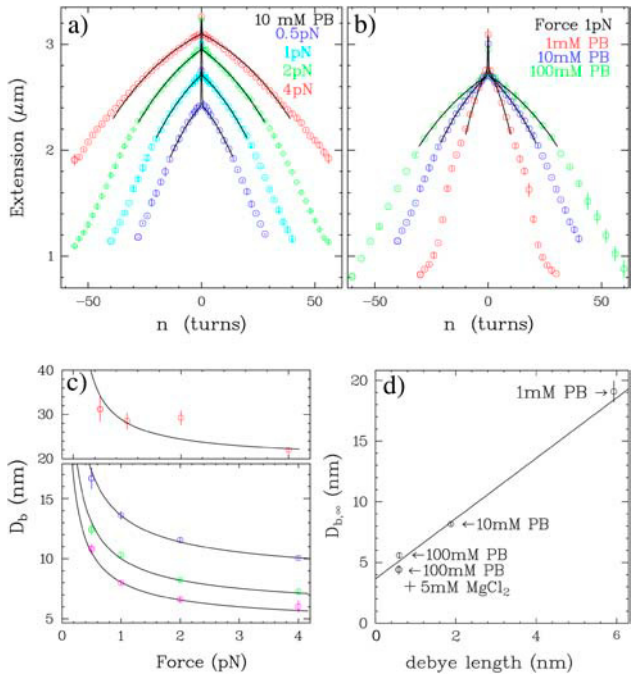

FIGURE 10 Dependence of the braid diameter D_b on force and ionic conditions. (*a*) Extension versus n curves in 10 mM phosphate buffer (*PB*) at different stretching forces and fits using the geometrical model (*solid lines*); red circle, 4 pN; green diamond, 2 pN; light-blue circle, 1 pN; and dark-blue circle, 0.5 pN. (*b*) Extension versus n curves at $F = 1$ pN and fits using the geometrical model (*solid lines*); red circle, 1 mM PB; light-blue circle, 10 mM PB; and dark-blue circle, 100 mM PB. (*c*) Evolution with the force of the fitted diameter of the braids D_b at different ionic concentrations: red circle, 1 mM PB; blue circle, 10 mM PB; green circle, 100 mM PB; and magenta circle, 100 mM PB + 5 mM $MgCl_2$. Error bars indicate the error (determined by bootstrap test) on the diameter fitted using the geometrical model. Following Marko (1997), D_b was fitted by $D_b = AF^{-3/4} + D_{b,\infty}$. (*d*) Evolution of $D_{b,\infty}$ (*circle*) with the Debye length of λ_D, calculated by Zhang et al. (2001) at the corresponding ionic concentration. Error bars indicate the error on $D_{b,\infty}$, which has been fitted using least-square methods. A linear fit yields $D_{b,\infty} = 2.5\ \lambda_D + 3.6$ nm.

force and can be computed from the variation of the braid's extension between $n = 0$ and $n = 1/2$. Fig. 9 *b* shows the value of $\Gamma(n)$ calculated for the parameters used in the simulations, see Fig. 7 *a*, ($2e/L_0 = 0.36$). The agreement between the geometric model and the simulation is very good. However, note that, because of the chains' fluctuations (that are neglected in the geometric model), there is a slight discrepancy near $n = 1/2$; the chains come into contact before $n = 1/2$, thus increasing the torque.

When $n > 1/2$, the computed torque $\Gamma(n)$ has a marked nonlinear dependence with n, which differs significantly from the results of the MC simulations (see Fig. 9 *c*). A possible reason for that discrepancy might be the finite persistence length of the braided chains, which would restrict their bending when the braid pitch is of similar size. The braid angle α in the model varies continuously until its buckling at $\alpha = 45°$, but the value of α deduced from the MC simulations (with persistence length $\xi = 50$ nm) varies little with n. Although this effect does not alter the variation of z with n, it does affect the estimation of the energetics of bending in the braiding regime and therefore the calculation of C_b.

THE COLLAPSE TRANSITION OF BRAIDS AT LOW SALT

The braiding of nicked DNA molecules in low salt conditions (≤10 mM PB) exhibits a surprising transition to a tight braided structure (Strick et al., 1998). Fig. 11 *a* shows that, in low salt, once the molecules have adopted the braided plectonemic structure described previously they may undergo a sharp hysteretic transition to a state with a larger extent and a much smaller decrease in extension upon braiding. In this regime, the extension varies much less per added turn ($dz/dn = 4$ nm/turns) than in the regime of (non-plectonemic) braids at small n ($dz/dn \approx 32$ nm/turns). The decrease in extension being proportional to the diameter of the braided structure, this result suggests that the intertwined molecules in the collapsed regime wound around each other in a structure much tighter than the regular braid between two dsDNAs. Since in the conditions of this experiment ($F = 2$ pN, 1 mM PB), the braid diameter $D_b = 25$ nm, see Fig. 10 *c*, we estimate by simple proportionality that the distance between the molecules in the collapse regime is $D_{coll} = D_b \times 4/32 \approx 3.1$ nm, which is close to the crystallographic diameter of DNA.

This collapse transition is observed for both right-handed ($n > 0$) and left-handed ($n < 0$) braids, although it appears to happen for a slightly smaller value of $|n|$ for left-handed turns. Surprisingly, this collapse is observed only in low salt conditions and not at high salt or in presence of Mg^{2+}, where one might have expected electrostatic repulsion to be weaker and the molecules to be closer to each other to begin with. The transition is reversible but highly hysteretic. The hysteresis is more pronounced for left- than for right-handed braids.

Fig. 11 *b* is a real-time recording of the transition to the collapsed state of a braid. The collapse occurred ~2 min after the molecules had been braided by $n = -35$ turns. Notice that the transition is very quick (although slower than our acquisition rate, 25 Hz) and that the molecules can be reversibly unbraided from the collapse regime by simply rotating the magnets back to zero. Analysis of the longitudinal fluctuations at $n = -26$ (data not shown) before and after the collapse transition showed that they decreased significantly after the transition, suggesting that the collapsed state is not only tighter but also stiffer than a regular braid (or a braid supercoil).

DISCUSSION

The braiding of two DNA molecules can be studied in great detail using a magnetic trap technique. Qualitatively and quantitatively the molecules respond to braiding as would the ropes in a twisted swing. Monte Carlo simulations of two braided WLC polymers fit the experimental data over the whole range of observation and confirm the transition to

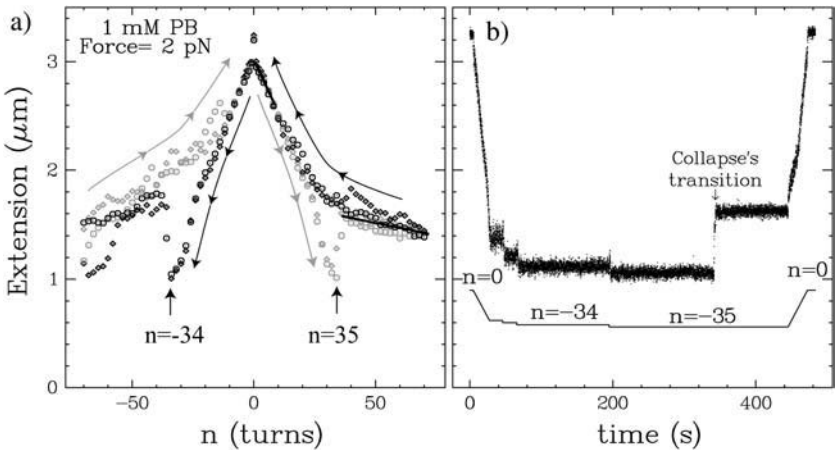

FIGURE 11 Torque-induced collapse of the braids. (*a*) Extension z versus catenation number (n) at 1 mM PB and $F = 2$ pN, with increasing (or *decreasing*) n shaded (or *open*) circles. At sufficiently high $|n|$ (in the plectonemic regime of braids), a hysteretic transition occurs (with a noticeable jump in extension; see *arrows* at $n = -34$ and $n = 35$) to a state characterized by a smaller decrease in extension per turn (Strick et al., 1998), dz/dn. In that state (i.e., for $|n| > 35$), $dz/dn \simeq 4$ nm/turn, whereas it is $\simeq 32$ nm/turn at small n. This observation suggests that the structure of braids in that state is very compact (with a braid diameter approximately eight times smaller than for small n). (*b*) Real-time observation of braid collapse. Recording of the extension z (*open squares*) and the set value of n (*continuous line*) as a function of time. Notice the quick and spontaneous increase in z at $n = -35$. Unlinking the molecules back to $n = 0$ reproduces the initial configuration.

plectonemes of braids at high braiding number. The elastic behavior of two braided polymers deduced from these simulations is also well fitted by the model of a twisted swing. As far as the experimental data is concerned, the length of each molecule is given by the extension of a WLC polymer under half the exerted tension, $F/2$. The diameter of the braid is set by the repulsive electrostatic and entropic interactions. The variation of the diameter with force is well fit by the predictions of Marko (1997), namely it decreases as $F^{-3/4}$ due to a reduction in entropic fluctuations at high forces. The electrostatic repulsion increases the DNA's effective diameter by an amount proportional, as expected, to the interaction range: the Debye length.

When the persistence length of the chains is comparable to the pitch of the braids, the numerical results show that the braid angle α differs from the predictions of our simple model. It saturates at an angle α_c less than the predicted value of 45° (data not shown). This numerical observation results from the stiffness of the chains that prevents them from bending as they wind around each other with an angle smaller than predicted. This effect due to the finite persistence length of the chains appears not to significantly affect the extension versus catenation behavior of braided chains, which may partly explain the good agreement between our simple geometric model and both MC simulations and experimental data. However, the difference observed between the torque expected from the geometric model and the one deduced from numerical simulation shows that the bending modulus of DNA, which is not taken into account in the geometric model, is important to understand the torque in DNA braids.

At large braiding number and in low salt conditions, we have observed a sudden transition to a structure still affected by the braiding of the molecules but with a decrease in extension per added turn corresponding to the molecules being a distance ~3.1-nm apart. It is surprising that such a transition is only observed in low salt conditions (1 mM PB and $F > 2$ pN or 10 mM PB and $F > 4$ pN), where electrostatic repulsive interactions have a much larger range ($\lambda_D \approx 6$ nm). It is probable that, in these conditions, the nicked DNA molecules are frayed, which may allow the single strands under tension to wind around each other in a tight, right- or left-handed, double-helical structure, as described on Fig. 12. This would explain the sharp transition observed when increasing the braiding number n as well as the smooth recovery to the initial structure when going back to $n = 0$. Note that the detailed structure of this braid greatly depends on the number of the nicks and their positions in the DNA molecule. Repeating the experiment with different sets of molecules lead to slightly different jumps in extension upon collapse as well as different braiding thresholds (data not shown). However, the experiment presented in Fig. 11 is the typical behavior of the braid observed in these conditions. A further study should investigate this transition quantitatively, using a well-defined specifically nicked construct. For example, it would be of great interest to determine the torque required to fray the molecules. Last, it has not escaped our notice that a critical test of the structure we suggest in Fig. 12 would be to try the relaxation of the single-strand braid by type Ia topoisomerase, which is known to operate single-strand passages. However, such a study is well beyond the scope of this article.

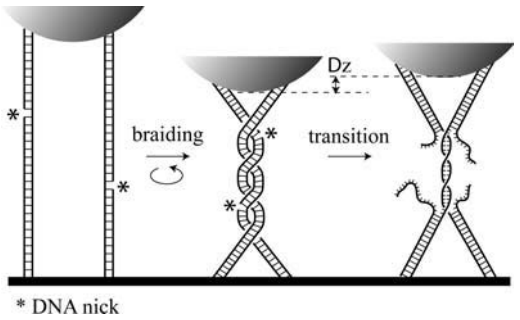

FIGURE 12 Model for the collapse transition observed in low ionic conditions. At small linking number, nicked double-stranded DNAs wrap around each other, thus reducing the system's extension (*center*). Beyond a critical linking number, the torque in the braids induces the melting of the molecules and the extrusion of single strands (*right*). The remaining (braided and stretched) single strands wind around each other in a helix that is tighter than the braid formed by two dsDNAs, thus increasing sharply the system's extension.

The results of the present experiments, simulations, and modeling shed new light on the structures (braids, plectonemes of braids, collapsed structures) possibly adopted by the catenated sister chromosomes in replication intermediates.

We acknowledge helpful discussions with J. Marko, J.-F. Allemand, S. Neukirch, and Y. Zhang and useful comments by the referees of this article. We also thank G. Lia for DNA constructs.

This work was supported for G.C., D.B., and V.C. by grants from Association de Recherche sur le Cancer, Centre National de la Recherche Scientifique, Ecole Normale Supérieure, Universities Paris VII and VI, European Union (''MolSwitch''), and for A.V. by the National Institutes of Health grant No. GM54215.

REFERENCES

Adams, D., E. Shekhtman, E. Zechiedrich, M. Schmid, and N. Cozzarelli. 1992. The role of topoisomerase IV in partitioning bacterial replicons and the structure of catenated intermediates in DNA replication. *Cell.* 71: 277–288.

Bouchiat, C., and M. Mézard. 1998. Elasticity theory of a supercoiled DNA molecules. *Phys. Rev. Lett.* 80:1556–1559.

Bryant, Z., M. D. Stone, J. Gore, S. B. Smith, N. R. Cozzarelli, and C. Bustamante. 2003. Structural transitions and elasticity from torque measurements on DNA. *Nature.* 424:338–341.

Charvin, G., V. Croquette, and D. Bensimon. 2003. Single molecule study of DNA unlinking by eukaryotic and prokaryotic type II topoisomerases. *Proc. Natl. Acad. Sci. USA.* 100:9820–9825.

Charvin, G., T. Strick, J.-F. Allemand, V. Croquette, and D. Bensimon. 2004. Twisting DNA: single molecules studies. *Contemp. Phys.* 45:383–403.

Cluzel, P., A. Lebrun, C. Heller, R. Lavery, J.-L. Viovy, D. Chatenay, and F. Caron. 1996. DNA: an extensible molecule. *Science.* 271:792–794.

Flyvbjerg, H., and H. G. Petersen. 1989. Error estimates on averages of correlated data. *J. Chem. Phys.* 91:461–466.

Frank-Kamenetskii, M., A. Lukashin, V. Anshelevich, and A. Vologoskii. 1985. Torsional and bending rigidity of the double helix from data on small DNA rings. *J. Biomed. Struct. Dyn.* 2:1005–1012.

Frank-Kamenetskii, M., and A. Vologodskii. 1981. Topological aspects of the physics of polymers: the theory and its biological applications. *Sov. Phys. Usp.* 24:679–696.

Klenin, K. V., A. V. Vologodskii, V. V. Anshelevich, A. M. Dykhne, and M. D. Frank-Kamenetskii. 1991. Computer simulation of DNA supercoiling. *J. Mol. Biol.* 217:413–419.

Leger, J. F., J. Robert, L. Bourdieu, D. Chatenay, and J. F. Marko. 1998. RecA binding to a single double-stranded DNA molecule: a possible role of DNA conformational fluctuations. *Proc. Natl. Acad. Sci. USA.* 95: 12295–12299.

Marko, J. 1997. Supercoiled and braided DNA under tension. *Phys. Rev. E.* 55:1758–1772.

Marko, J. 1999. Coupling of intramolecular and intermolecular linkage complexity of two DNAs. *Phys. Rev. E.* 59:900–912.

Marko, J., and E. Siggia. 1995. Statistical mechanics of supercoiled DNA. *Phys. Rev. E.* 52:2912–2938.

Meselson, M., and F. W. Stahl. 1958. The replication of DNA. *Cold Spring Harb. Symp. Quant. Biol.* 23:9–12.

Metropolis, N., A. Rosenbluth, M. Rosenbluth, and A. Teller. 1953. Simulated annealing. *J. Chem. Phys.* 21:1087–1092.

Moroz, J., and P. Nelson. 1998a. Entropic elasticity of twist-storing polymers. *Macromolecules.* 31:6333–6347.

Moroz, J., and P. Nelson. 1998b. Torsional directed walks, entropic elasticity and DNA twist stiffness. *Proc. Natl. Acad. Sci. USA.* 94: 14418–14422.

Neukirch, S. 2004. Extracting DNA-twist rigidity from experimental supercoiling data. *Phys. Rev. Lett.* 93:198107-1–198107-2.

Neukirch, S., and G. van der Heidjen. 2002. Geometry and mechanics of uniform *N*-plies: from engineering ropes to biological filaments. *J. Elast.* 69:41–72.

Rybenkov, V., N. Cozzarelli, and A. Vologodskii. 1993. Probability of DNA knotting and the effective diameter of the DNA double-helix. *Proc. Natl. Acad. Sci. USA.* 90:5307–5311.

Rybenkov, V., C. Ullsperger, A. Vologodskii, and N. Cozzarelli. 1997. Simplification of DNA topology below equilibrium values by type II topoisomerases. *Science.* 277:690–693.

Schvartzman, J. B., and A. Stasiak. 2004. A topological view of the replicon. *EMBO J.* 5:256–261.

Stigter, D. 1977. Interactions of highly charged colloidal cylinders with applications to double-stranded DNA. *Biopolymers.* 16:1435–1448.

Stone, M. D., Z. Bryant, N. J. Crisona, S. B. Smith, A. Vologodskii, C. Bustamante, and N. R. Cozzarelli. 2003. Chirality sensing by *Escherichia coli* topoisomerase IV and the mechanism of type II topoisomerases. *Proc. Natl. Acad. Sci. USA.* 100:8654–8659.

Strick, T., J. Allemand, D. Bensimon, A. Bensimon, and V. Croquette. 1996. The elasticity of a single supercoiled DNA molecule. *Science.* 271:1835–1837.

Strick, T., J.-F. Allemand, D. Bensimon, and V. Croquette. 1998. The behavior of supercoiled DNA. *Biophys. J.* 74:2016–2028.

Vologodskii, A. 1994. DNA extension under the action of an external force. *Macromolecules.* 27:5623–5625.

Vologodskii, A., and N. Cozzarelli. 1995. Modeling of long-range electrostatic interactions in DNA. *Biopolymers.* 35:289–296.

Vologodskii, A., and M. Frank-Kamenetskii. 1992. Modeling supercoiled DNA. *Methods Enzymol.* 211:468–472.

Vologodskii, A., A. Lukashin, and M. Frank-Kamenetskii. 1975. Topological interactions between polymer chains. *Sov. Phys. JETP.* 40: 932–936.

Vologodskii, A., and J. Marko. 1997. Extension of torsionally stressed DNA by external force. *Biophys. J.* 73:123–132.

Vologodskii, A. V., and N. R. Cozzarelli. 1996. Effect of supercoiling on the juxtaposition and relative orientation of DNA sites. *Biophys. J.* 70: 2548–2556.

Vologodskii, A. V., W. Zhang, V. V. Rybenkov, A. A. Podtelezhnikov, D. Subramanian, J. D. Griffith, and N. R. Cozzarelli. 2001. Mechanism of topology simplification by type II DNA-topoisomerases. *Proc. Natl. Acad. Sci. USA.* 98:3045–3049.

Wang, J. C. 2002. Cellular roles of DNA topoisomerases: a molecular perspective. *Nat. Rev. Mol. Cell Biol.* 3:430–440.

Wang, M., M. Schnitzer, H. Yin, R. Landick, J. Gelles, and S. Block. 1998. Force and velocity measured for single molecules of RNA polymerase. *Science.* 282:902–907.

Watson, J., and F. Crick. 1953. Molecular structure of nucleic acids: a structure for deoxyribose nucleic acid. *Nature.* 171:737–738.

Zhang, Y., H. Zhou, and Z.-C. Ou-Yang. 2001. Stretching single-stranded DNA: interplay of electrostatic, basepairing, and base-stacking interactions. *Biophys. J.* 81:1133–1143.